Available online at www.sciencedirect.com
ScienceDirect
Materials Science and Engineering C 27 (2007) 729–735
MATERIALS SCIENCE & ENGINEERING C
www.elsevier.com/locate/msec

Hydroxyapatite nanopowders: Synthesis, densification and cell–materials interaction

Ashis Banerjee, Amit Bandyopadhyay, Susmita Bose *

W. M. Keck Biomedical Materials Research Laboratory, School of Mechanical and Materials Engineering, Washington State University, Pullman, WA 99164-2920, United States

Received 17 January 2006; received in revised form 7 July 2006; accepted 10 July 2006
Available online 22 August 2006

Abstract

Hydroxyapatite (HA) nanopowders with different aspect ratios were synthesized using reverse micelle template system. Nanopowders were characterized using X-ray diffraction (XRD), BET specific average surface area analysis and transmission electron microscopy (TEM). It was observed that increase in aqueous to organic ratio (A/O) and pH decreased the aspect ratio of the nanopowders. HA nanopowders with the highest aspect ratio (rod-shaped) of 7.2±3.2 and the lowest aspect ratio (spherical) of 1.3±0.3 were synthesized for processing dense compacts. Effect of powder morphology on densification at 1250 °C was studied with different amount of rod-shaped and spherical nanopowders. It was observed that an increase in high aspect ratio powder content in the compacts decreased sintered density under pressureless sintering condition. Also, due to excessive grain growth, no nanoscale morphology could be retained in the sintered microstructure. Mineralization study in simulated body fluid (SBF) showed formation of apatite layer on the entire surface of both compacts made with spherical and rod-shaped particles. Cytotoxicity result with OPC1 human osteoblast cells showed excellent cell attachment and cell spreading on samples after 5 days in culture.

Keywords: Hydroxyapatite; Nanopowder; Synthesis; Sintering; Apatite layer; Human osteoblast cells

1. Introduction

Hydroxyapatite (HA, $Ca_{10}(PO_4)_6(OH)_2$) is the principal inorganic constituent of bones and teeth [1]. Synthetic HA has excellent biocompatibility and bioactivity, and widely used in many biomedical applications such as non-load bearing implants and coating onto prostheses [2,3]. For successful application of HA based ceramics as bone grafts, higher strength and toughness are desirable. Unfortunately, because of poor sinterability, HA ceramics show low strength and toughness, especially in wet environment under physiological condition, which makes them unsuitable even for low load bearing applications. Nanostructured material can improve the sinterability due to high surface energy and, therefore, improve mechanical properties [4]. But sintering behavior not only depends on particle size but also on particle size distribution and morphology of the powder particles [5]. Large particle size along with hard agglomerates exhibits lower densification in HA [6]. Difference in shrinkage between the agglomerates is also responsible to produce small cracks in the sintered HA [7]. Therefore, synthesis of agglomerate free or soft agglomerated nanostructured HA can be an important step to achieve good mechanical properties for dense nanostructure.

Various synthesis methods of HA have been reported, including solid-state reaction [8], sol–gel synthesis [9,10], pyrolysis of aerosols [11], hydrothermal reaction [12] and microemulsion [13,14]. The degree of success of these methods, in preparing HA, differs significantly from one to the other. Microemulsion has been shown to be one of the few techniques, which can give nanoparticles with minimum agglomeration [15]. Several researchers have reported synthesis of HA nanopowders by microemulsion and reverse micelle method using different surfactants such as mixed poly(oxyethylene)$_5$nonyl phenol ether (NP5) and poly(oxyethylene)$_9$nonyl phenol ether (NP9) [16,17],

* Corresponding author. Tel.: +1 509 335 7461.
E-mail address: sbose@wsu.edu (S. Bose).

0928-4931/$ - see front matter © 2006 Elsevier B.V. All rights reserved.
doi:10.1016/j.msec.2006.07.010

cetyltrimethylammonium bromide (CTAB) [18]. In our previous work, we have [19] reported synthesis of HA nanopowder by emulsion using mixed poly(oxyethylene)$_5$nonylphenol ether (NP5) and poly(oxyethylene)$_{12}$noylphenol ether (NP12) as surfactants and cyclohexane as oil phase. The starting materials Ca$(NO_3)_2$ and H_3PO_4 were used as Ca^{2+} and PO_4^{3-} source. Size of the particles was below 100 nm and as the aqueous to organic ratio increased the aspect ratio of the particles decreased.

In this research, HA nanopowders with controlled morphology were synthesized with poly(oxyethylene)$_5$nonylphenol ether (NP5) and poly(oxyethylene)$_{12}$nonylphenol ether (NP12) as surfactants and cyclohexane as an organic solvent. The highest aspect ratio (rod-shaped particles) of 7.2±3.2 and the lowest aspect ratio (spherical) of 1.3±0.3 were synthesized for processing dense compacts. Varying amounts of rod-shaped particles were added in the spherical nanopowder to process green compacts. Sintering was done at 1250 °C for 3 h. Density, microhardness and indentation fracture toughness were measured on sintered compacts. Apatite formation in SBF and *in vitro* cell–materials interaction with OPC1 cells were studied as a part of biological property evaluation.

2. Experimental

2.1. Materials

Calcium nitrate ($Ca(NO_3)_2{\cdot}4H_2O$, J. T. Baker, NJ) and orthophosphoric acid (H_3PO_4, Fisher Scientific, NJ) were used as source of Ca^{2+} ion and PO_4^{3-} ion. Cyclohexane (Fisher Scientific, NJ) was used as organic solvent and poly(oxyethylene)$_5$nonylphenol ether (NP5) and poly(oxyethylene)$_{12}$nonylphenol ether (NP12) (Aldrich, WI) were used as surfactants. Ammonium hydroxide (NH_4OH, 28–30%, J. T. baker, NJ) was used to adjust the pH of the emulsion system.

2.2. Synthesis of nanopowders

HA nanopowders were synthesized using a standard method established as described in Ref. [19]. 5 M aqueous solution of Ca^{2+} ion was prepared by dissolving 0.01 mol (2.3615 g) of Ca$(NO_3)_2{\cdot}4H_2O$ in 2 ml distilled water. 0.006 mol (0.689 g) of phosphoric acid was added to the system to maintain a Ca to P molar ratio of 1.67:1. The organic phase was prepared by adding required amount of surfactant in cyclohexane with vigorous stirring. Low aspect ratio HA nanopowder was prepared using NP12 surfactant. 10 vol.% NP12 was dissolved in cyclohexane and the aqueous phase with the organic phase was mixed in the ratio of 1:15 with vigorous stirring. High aspect ratio HA nanopowder was prepared by using NP5 surfactant. 10 vol.% NP5 was dissolved in cyclohexane and the aqueous phase with the organic phase was mixed in the ratio of 1:5 with vigorous stirring. Nanopowders were synthesized at pH 7 and 9, with addition of NH_4OH, to study the effect of pH on powder morphology. All reactions were aged for 24 h at room temperature. After aging, the emulsion was evaporated on the hot plate at 150 °C followed by complete drying at 450 °C. The dry precursor powder was calcined at 650 °C for 2 h to get carbon free crystalline HA nanopowder. Fig. 1 shows the synthesis steps of nanopowder preparation.

2.3. Processing of HA compacts

To study the effect of nanopowder morphology on densification, varying amounts of rods (0 to 100 wt.%) were added in spherical nanopowder to process dense compacts. Acetone was added in the mix and ultrasonicated for 30 min for homogenous mixing. After mixing, acetone was evaporated by heating at 200 °C for 1 h on a hot plate. Dried powders were pressed using a uniaxial press, and sintered at 1250 °C for 3 h in a muffle furnace.

2.4. Characterization

2.4.1. Nanopowder characterization

Nanopowders were characterized for their phase purity using X-ray diffraction (XRD) with a Philips PW 3040/00 X'pert MPD system at room temperature with Co-K_{α} radiation and an Ni-filter over the 2θ range of 20° to 70° at a step size of 0.02° (2θ) and a count time of 0.5 s/step. The specific average surface area measurement was done using a five point BET surface area analysis (Tristar 3000, Micromeritics, GA). Powder morphology and particle size was evaluated using a transmission electron microscope (JEOL, JEM 120, MA).

2.4.2. Physical and mechanical characterization of HA compacts

Sintered HA compacts were characterized for their density, microhardness and indentation fracture toughness. Microhardness

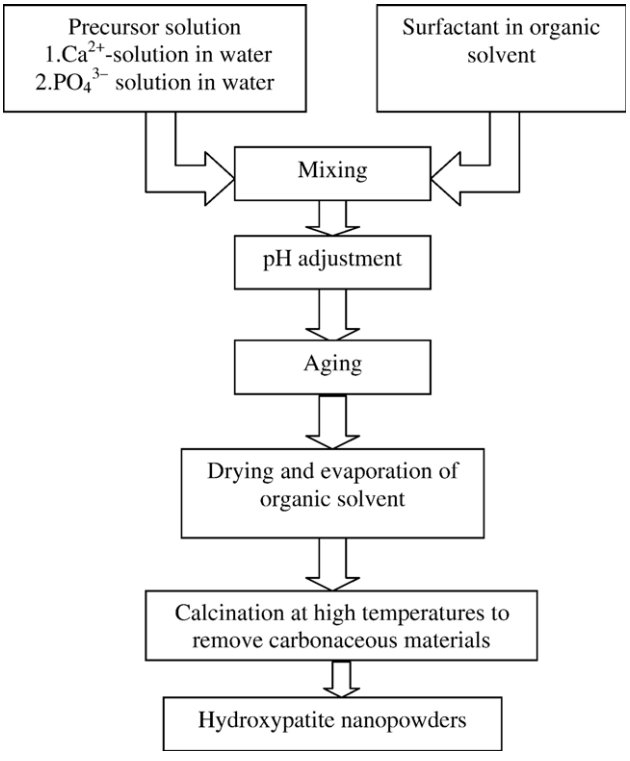

Fig. 1. Synthesis of hydroxyapatite nanopowder by reverse micelle method.

measurement was done with a Vicker's indenter. Indentation fracture toughness was calculated from the indentation mark and crack length using the equation [20]

$$\text{Fracture toughness}(K_{IC}) = 0.016 \times (E/H)^{1/2} \times P/C^{3/2}$$

where E is Young's modulus of the sample, H is microhardness in GPa, P is load applied and C is 1/2 of crack length.

2.4.3. In vitro biological characterization

2.4.3.1. Mineralization behavior under simulated body fluid (SBF). Mineralization behavior in SBF was studied by keeping samples in SBF up to 28 days. To study the effect of powder morphology on the apatite formation on sample surface, 100% spherical and 100% rod-shaped content sintered samples were used. SBF was prepared by dissolving reagent-grade chemicals of NaCl, $NaHCO_3$, KCl, $K_2HPO_4{\cdot}3H_2O$, $MgCl_2{\cdot}6H_2O$, $CaCl_2$ and Na_2SO_4 into distilled water and buffering at pH 7.35 with tris(hydroxymethyl)aminomethane ($(CH_2OH)_3CNH_3$) and 1.0 M hydrochloric acid at room temperature [21]. Each sample was kept in 10 ml of SBF solution. Every 4 days interval, SBF solution was changed with freshly made solution. After 28 days, the samples were taken out, washed and dried at 150 °C for 24 h. After complete drying, samples were observed under SEM to study apatite layer formation.

2.4.3.2. Cell attachment behavior. *In vitro* analyses were carried out using a modified human osteoblast (HOB) cell line (OPC1). OPC1 is a conditionally immortalized osteoprecursor cell line derived from human fetal bone tissue [22]. OPC1 cells were cultured in a standard medium made of McCoy's 5A (with L-glutamine, without phenol red and sodium bicarbonate) [Sigma Chemical Co, Saint Louis, MO, USA], supplemented with10% fetal bovine serum, 2.2 g/l sodium bicarbonate, 0.1 g/l penicillin and 0.1 g/l streptomycin and 8 μg/ml Fungizone (Gibco Laboratories, Grand Island, NY). Cells were removed from cell culture dishes with trypsin and split into 1:2 ratio, 3 days prior to use. Samples were sterilized via autoclaving and then seeded with OPC1 cells and cultured under standard aseptic conditions. After 5 days, samples were dried, stained and observed under SEM.

3. Results and discussion

Addition of NP5 or NP12 in cyclohexane formed small polar cores by organizing the polar head groups away from non-polar organic solvents. When aqueous solutions of $Ca(NO_3)_2$ and H_3PO_4 were added in that organic phase, water went to the small polar cores and formed microreactors. All reactions were carried out at pH 7 or above, and aged for 24 h at room temperature. The ratio of Ca^{2+} and PO_4^{3-} ions in aqueous solution was maintained at 1.67 because in HA, Ca to P ratio is 1.67. Addition of NH_4OH increased the pH of the system. An

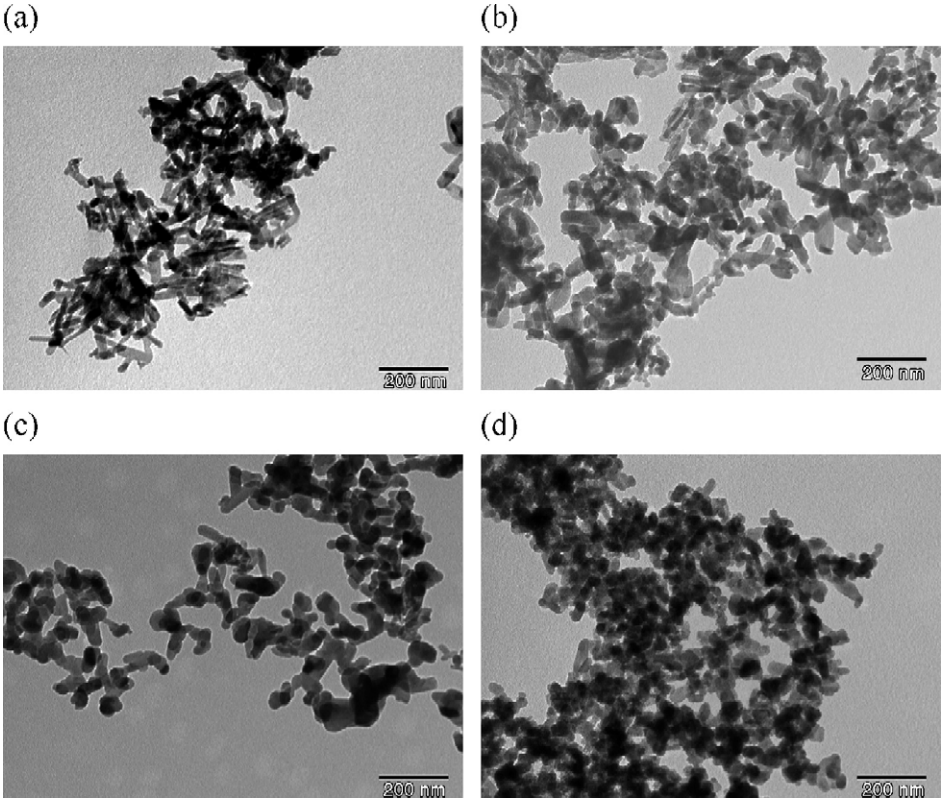

Fig. 2. TEM analysis of HA nanopowders calcined at 650 °C (a) with NP5 at pH 7 and A/O ratio of 1:5, (b) with NP5 at pH 9 and A/O ratio of 1:5, (c) with NP12 at pH 7 and A/O ratio of 1:15 and (d) with NP12 at pH 9 and A/O ratio of 1:15.

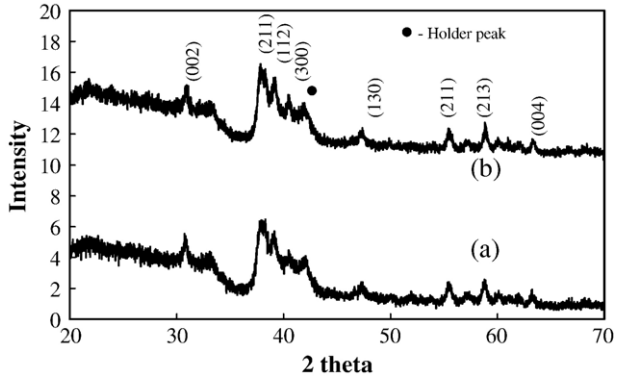

Fig. 3. XRD of the synthesized HA nanopowder and calcined at 650 °C (a) with NP5 at pH 7 and aqueous to organic ratio of 1:5 and (b) with NP12 at pH 9 and aqueous to organic ratio of 1:15.

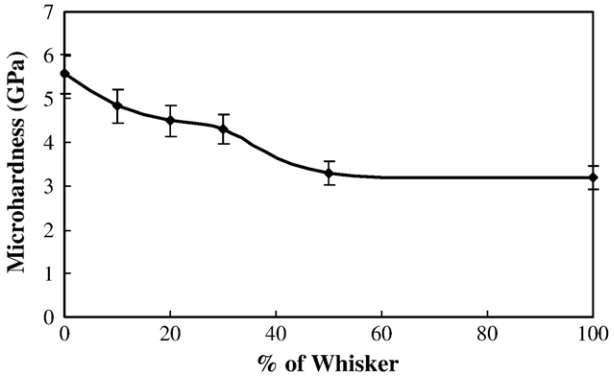

Fig. 5. Effect of rod-shaped (whisker) particle addition on microhardness of sintered HA compacts.

increase in pH helped in precipitation and formation of hydroxyapatite ($Ca_{10}(PO_4)_6(OH)_2$) phase. The overall reaction is given below.

$$10Ca^{2+} + 6PO_4^{3-} + 2OH^- = Ca_{10}(PO_4)_6(OH)_2$$

$$10Ca(NO_3)_2 + 6H_3PO_4 + 2NH_4OH = Ca_{10}(PO_4)_6(OH)_2 + 2NH_4NO_3 + 18HNO_3$$

All powders were calcined at 650 °C for 2 h to remove carbonaceous materials and promote crystallization of HA.

Fig. 2 shows the bright field TEM image of nanopowders, synthesized at different conditions. Fig. 2a and b shows the effect of pH on nanopowder morphology synthesized using NP5 with A/O ratio of 1:5. Increase in pH from 7 to 9 decreased the aspect ratio of nanopowders from 7.2±3.2 to 3.5±1.0. Fig. 2c and d shows effect of pH on nanopowder morphology using NP12 with A/O ratio of 1:15. It was observed that increase in pH from 7 to 9 decreased the aspect ratio of nanopowder from 2.4±0.9 to 1.3±0.3. Increase of pH by addition of NH_4OH increased OH^- ion concentration in the polar core and gave repulsive effect which decreased aspect ratio of the polar core and resulted decrease in the aspect ratio of the synthesized nanopowder. A detail study on the effect of A/O ratios and pH on nanopowders morphology was done using NP5 and NP12. Effect of A/O ratio on nanopowder morphology was studied at A/O ratios of 1:5, 1:10 and 1:15 in both pH 7 and 9. It was observed that at lower A/O ratio and pH aspect ratio of the nanopowders was high. As the A/O ratio or pH increased, aspect ratio was decreased. At a particular A/O ratio and pH, aspect ratio of the nanopowder synthesized using NP5 was higher than that of using NP12.

To study the aspect ratio effect on densification, highest aspect ratio nanopowder or rod-shaped particles synthesized using NP5 with A/O ratio of 1:5 and pH 7 (aspect ratio of 7.2±3.2) and lowest aspect ratio or spherical nanopowder synthesized using NP12 with A/O ratio of 1:15 and pH 9 (aspect ratio of 1.3±0.3) were used. Densification was studied by mixing different amounts of rod-shaped particles in spherical nanopowders. As densification depends on surface area, therefore, surface area of the nanopowders was measured at different rod-shaped particle levels. Specific average surface areas of as-synthesized spherical and rod-shaped HA powders were 39 m^2/g and 29 m^2/g, respectively. It was observed that addition of HA rod-shaped particles decreased the surface area of the mixture following the rule of mixture. Fig. 3 shows XRD analysis of the synthesized nanopowders. It was observed that phase pure HA nanopowders were obtained in all cases. It was found that type of surfactant or aqueous to organic ratio did not influence phase formation.

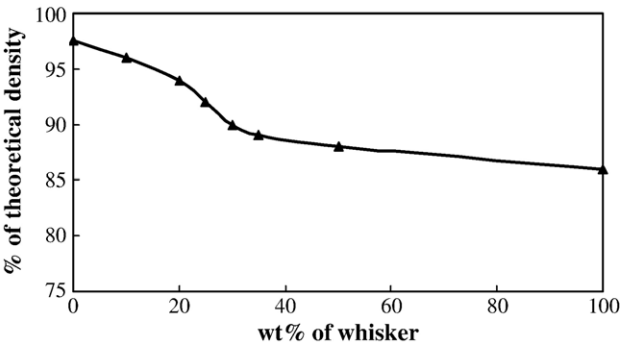

Fig. 4. Densification behavior of HA compacts at 1250 °C for 3 h with different rod-shaped (whisker) particle content.

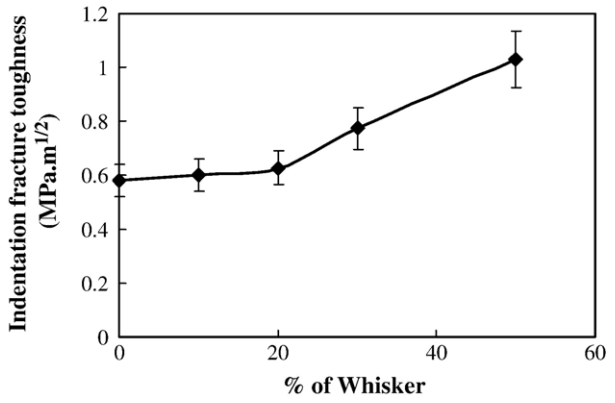

Fig. 6. Effect of rod-shaped (whisker) particle addition on indentation fracture toughness of sintered HA compacts.

3.1. Physical and mechanical properties

Fig. 4 shows the effect of rod-shaped particle addition on densification of spherical nanopowder. It was observed that increase in rod-shaped particles content decreased the density of the sintered sample. Spherical nanopowders have higher surface energy per unit volume compared to rod-shaped particles. Addition of rod-shaped particles decreased the overall surface energy of the system, which is the driving force for solid state sintering, and reduced the densification rate. Sintering plot shows three distinct regions with different slopes. During the initial part, up to 20 wt.% rod-shaped particle, densification rate slowly decreased linearly with rod-shaped particle addition. Densification in this zone was primarily controlled by the spherical powders and their distribution. 20–30 wt.% rod-shaped particles content was a transitional zone, where densification rate control changed from spherical to rod-shaped particles. Above 30 wt.% rod-shaped particles, densification kinetics was very slow and was controlled by the rod-shaped particles. In all cases, sintered microstructure did not show any rod-shaped particles in the final structure of these nanopowders due to grain growth.

Fig. 5 shows the effect of rod-shaped particle addition on microhardness. The highest microhardness of 5.5 GPa was obtained for dense compacts made with 100% spherical nanopowder. It was observed that an increase in rod-shaped particle amount decreased microhardness of the sintered compacts and the lowest microhardness of 3.4 GPa was obtained with dense compacts made from 100% nanorod-shaped particle sample. The curve followed the similar profile as the density plot which suggests that variation in microstructure was due to the residual porosity in the sample.

Fig. 6 shows the effect of rod-shaped particle addition on indentation fracture toughness. Compacts of 100% spherical HA nanopowder showed the lowest fracture toughness of 0.6 MPa/m^2. It was observed that after 20 wt.% rod-shaped particle addition, fracture toughness increased linearly with rod-

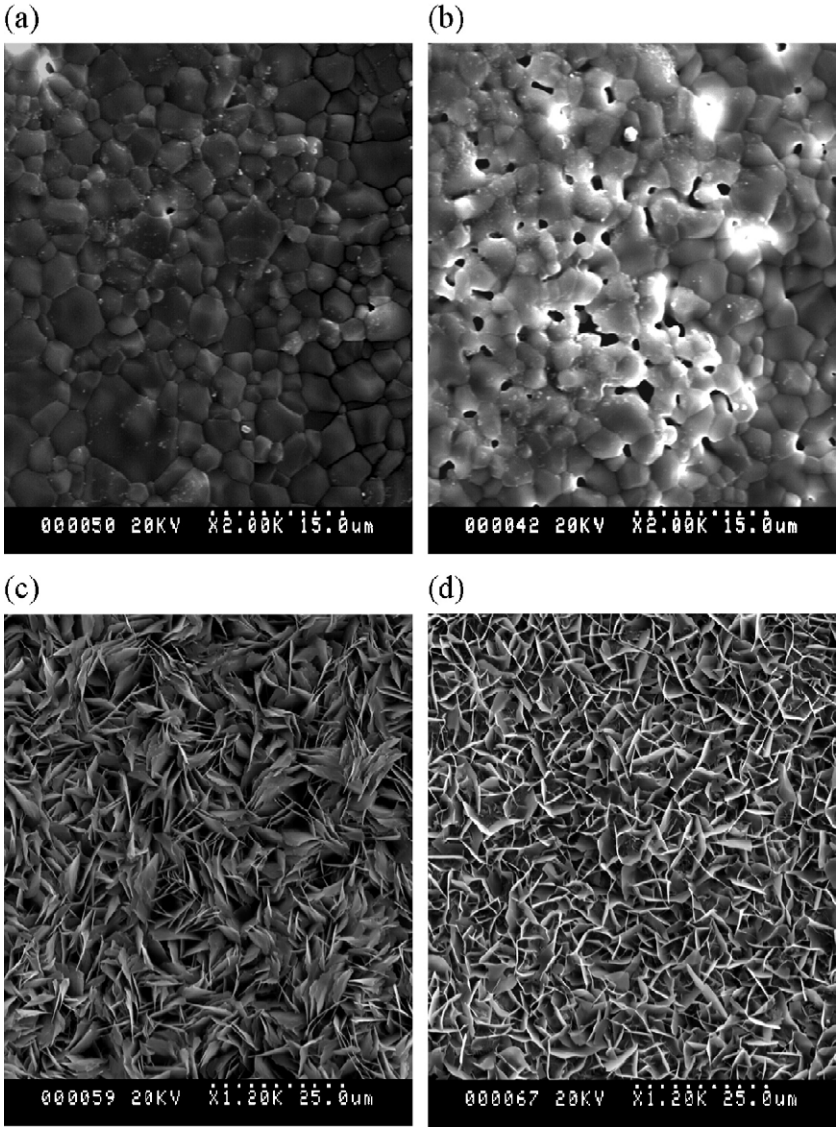

Fig. 7. Top surface SEM micrograph of dense HA compacts. (a, b) As processed and (c, d) 28 days in SBF. For (a) and (c), 100% spherical nanopowder was used as starting material. For (b) and (d), 100% rod-shaped particles were used as starting material.

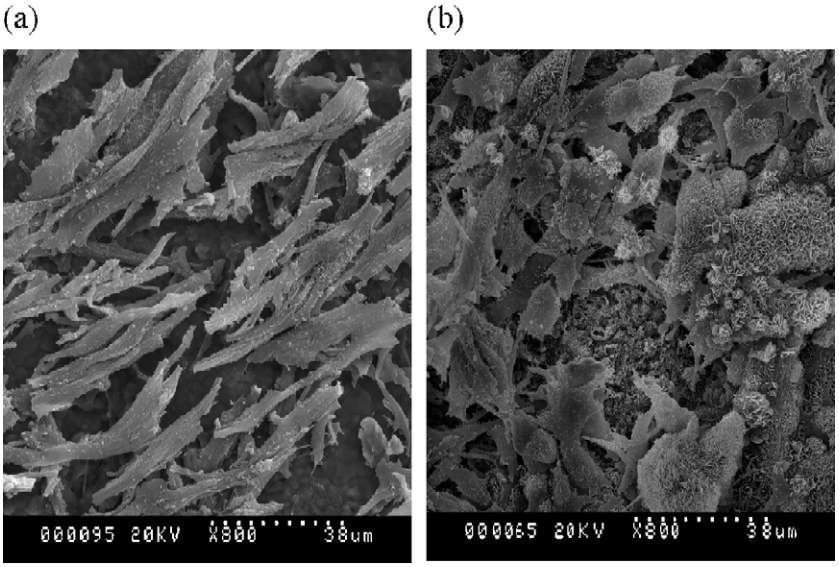

Fig. 8. *In vitro* cell–materials interaction after 5 days with OPC 1 cells. (a) OPC1 cells on dense HA processed with 100% spherical nanopowders and (b) OPC1 cells on dense HA processed with 100% rod-shaped particles.

shaped particle addition. At 50 wt.% rod-shaped particles, a fracture toughness of 1 MPa/m^2 was obtained. SEM micrograph showed that addition of rod-shaped particles increased porosity of the sintered samples, which limited the crack propagation, and thus increased indentation fracture toughness.

The present study showed that the morphology of nanopowder had effect on densification, microstructure and mechanical properties. However, rod-shaped morphology and nanosized grains could not be retained in the final microstructure due to grain growth. Nanosized rod-shaped particles embedded in nanosized grains in the sintered compacts can significantly improve mechanical properties of these compacts. Sintering at lower temperature or microwave sintering can reduce the grain growth. Cold isostatic pressing (CIP) can improve the green density of these compacts and thus can reduce sintering temperature. Currently we are investigating how to control densification and microstructure to improve mechanical properties in the final structure using these processes.

3.2. Cell–materials interactions

Fig. 7 shows the effect of densification on mineralization of HA compacts. It was observed that with 100% spherical nanopowder and 100% rod-shaped particle samples, uniform apatite layer was formed on the surface of the compacts. This is in line with the observation made by several research groups [23,24]. Compact made with spherical nanopowder showed denser apatite layer formation on the surface compared to compact made with pure rod-shaped particles after 28 days in SBF. Mechanism of apatite deposition was studied by several researchers [23,25]. They observed that after a short period of time amorphous calcium phosphate (ACP) deposited on the surface of dense HA compacts, but after a few days ACP converted to apatite by chemical reaction [23–25].

Fig. 8 shows cytotoxicity and cell attachment behavior of the HA compacts. In both cases, excellent cell–materials interactions with some newly formed apatite were observed as cells were spread well on the surfaces. Good cell–cell interactions can also be observed.

4. Conclusions

HA nanopowder with controlled morphology was synthesized using reverse micelle method. Spherical HA nanopowder with aspect ratio of 1.3±0.3 was synthesized using NP12 surfactant. Nanosized HA rod-shaped particles with aspect ratio of 7.2±3.2 was synthesized using NP5 surfactant. Addition of rod-shaped particles decreased the density of sintered samples. Microhardness was decreased due to the addition of rod-shaped particles. Indentation fracture toughness increased with rod-shaped particle addition to the spherical nanopowder. Microstructural analysis showed that no rod-shaped particle was present in the sintered compacts due to excessive grain growth at 1250 °C for 3 h. Samples in SBF showed formation of dense apatite layer on all samples. Cytotoxicity results with OPC1 cells showed excellent cell attachment for all samples.

Acknowledgments

The authors would like to acknowledge Ms. Jessica Moore and Prof. Howard L. Hosick for experimental support with the cytotoxicity tests. The authors would like to thank the National Science Foundation for the financial support under the Presidential CAREER Award for Scientists and Engineers (PECASE) to Dr. S. Bose (CTS # 0134476) for this work.

References

[1] L. Hench, J. Am. Ceram. Soc. 74 (1998) 1487.
[2] K. de Groot, Biomaterials 1 (1980) 47.
[3] F.H. Lin, C.C. Lin, H.C. Lu, Y.Y. Huang, C.Y. Wang, C.M. Lu, Biomaterials 15 (1984) 1087.

[4] W.D. Kingery, H.K. Bowen, D.R. Uhlmann, In: Introduction to Ceramics, Second ed., John Wiley and Sons, 1976, p. 469.
[5] A. Banerjee, S. Bose, Chem. Mater. 16 (26) (2004) 5610.
[6] M.G.S. Murray, J. Wang, C.B. Ponton, P.M. Marquis, J. Mater. Sci. 30 (1995) 3061.
[7] A.J. Ruys, M. Wei, C.C. Sorrel, M.R. Dickson, A. Brandwood, B.K. Milthpore, Biomaterials 16 (1995) 409.
[8] R.R. Rao, H.N. Roopa, T.S. Kanan, J. Mater. Sci., Mater. Med. 8 (1997) 511.
[9] A. Deptula, W. Lada, T. Olczak, A. Borello, C. Alvani, A. Dibartolomeo, J. Non-Cryst. Solids 147 (1992) 537.
[10] S. Bose, S.K. Saha, J. Am. Ceram. Soc. 86 (60) (2003) 1055.
[11] M. Valet-Regi, M.T. Gutierrez-Rios, M.P. Alonso, M.I. De Frutos, S. Nicolopoulos, J. Solid State Chem. 112 (1994) 58.
[12] H. Hattori, Y. Iwadate, J. Am. Ceram. Soc. 73 (1990) 1803.
[13] G.K. Lim, J. Wang, S.C. Ng, C.H. Chew, L.M. Gan, Biomaterials 18 (1997) 1433.
[14] K. Sonoda, T. Furuzono, D. Walsh, K. Sato, J. Tanaka, Solid State Ionics 151 (2002) 321.
[15] M.P. Pileni, J. Phys. Chem. 97 (1993) 6961.
[16] G.K. Lim, J. Wang, S.C. Ng, L.M. Gan, Mater. Lett. 28 (1996) 431.
[17] G.K. Lim, J. Wang, S.C. Ng, C.H. Chew, L.M. Gan, Biomaterials 18 (1997) 1433.
[18] Y. Liu, W. Wang, Y. Zhan, C. Zheng, G. Wang, Mater. Lett. 56 (2002) 496.
[19] S. Bose, S.K. Saha, Chem. Mater. 15 (2003) 4464.
[20] G.R. Anstis, P. Chantikul, B.R. Lawn, D.B. Marshall, J. Am. Ceram. Soc. 64 (9) (1981) 533.
[21] T. Kokubo, H. Kushitani, S. Sakka, T. Kitsugi, T. Yamamuro, J. Biomed. Mater. Res. 24 (1990) 721.
[22] S.R. Winn, G. Randolph, H. Uludag, S.C. Wong, G.A. Hair, G.O. Hollinger, J. Bone Miner. Res. 14 (1999) 1.
[23] Y.W. Gu, K.A. Khor, P. Cheang, Biomaterials 25 (2004) 4127.
[24] H.M. Kim, T. Himeno, T. Kokubo, T. Nakamura, Biomaterials 26 (2005) 4366.
[25] X. Lu, Y. Leng, Biomaterials 26 (2005) 1097.